Heliyon 10 (2024) e39073

Contents lists available at ScienceDirect

Heliyon

journal homepage: www.cell.com/heliyon

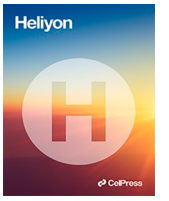

Research article

Hyperthermia and biological investigation of a novel magnetic nanobiocomposite based on acacia gum-silk fibroin hydrogel embedded with poly vinyl alcohol

Zeinab Pajoum [a], Hooman Aghamirza Moghim Aliabadi [b], Adibeh Mohammadi [c], Zahra Sadat [c], Amir Kashtiaray [c], Milad Salimi Bani [d], Mohammadali Shahiri [e], Mohammad Mahdavi [f], Reza Eivazzadeh-Keihan [c,**], Ali Maleki [c,*], Majid M. Heravi [a,***]

[a] *Department of Chemistry, School of Physics and Chemistry, Alzahra University, PO Box 1993891176, Vanak, Tehran, Iran*
[b] *Advanced Chemical Studies Lab, Department of Chemistry, K. N. Toosi University of Technology, Tehran, Iran*
[c] *Catalysts and Organic Synthesis Research Laboratory, Department of Chemistry, Iran University of Science and Technology, Tehran, 16846-13114, Iran*
[d] *Department of Optics and Photonics, Wroclaw University of Science and Technology, Wroclaw, Poland*
[e] *Department of Biomedical Engineering, Amirkabir University of Technology, Tehran, Iran*
[f] *Endocrinology and Metabolism Research Center, Endocrinology and Metabolism Clinical Sciences Institute, Tehran University of Medical Sciences, Tehran, Iran*

ARTICLE INFO

Keywords:
Acacia hydrogel
Silk fibroin
Biological activity
Hyperthermia
Poly vinyl alcohol

ABSTRACT

The design and synthesis of biocompatible nanostructures for biomedical applications are considered vital challenges. Herein, a nanobiocomposite based on acacia hydrogel, natural silk fibroin protein, and synthetic protein fibers of polyvinyl alcohol was fabricated and magnetized with iron oxide nanoparticles (Fe_3O_4 MNPs). The structural properties of the hybrid nanobiocomposite were investigated by essential analyses such as Fourier Transform Infrared Spectrometer (FTIR), Field emission scanning electron microscopy (FE-SEM), and X-ray powder diffraction)XRD(analyses, Thermogravimetric and Differential thermogravimetric analysis (TGA-DTG), Vibrating-sample magnetometry (VSM), and Energy Dispersive X-Ray Analysis (EDX). The biological activities and functional properties of the prepared magnetic nanobiocomposite were studied. Results proved that this nanobiocomposite is non-toxic to the healthy HEK293T cell line. In addition, the synthesized nanobiocomposite showed an approximately 22 % reduction in cell viability of BT549 cells after 72 h. All results confirmed the anti-cancer properties of nanobiocomposite against breast cancer cell lines. Therefore, the prepared nanobiocomposite is an excellent material that can use for in-vivo application. Finally, the hyperthermia application was evaluated for this nanobiocomposite. The SAR was measured 93.08 (W/g) at 100 kHz.

* Corresponding author.
** Corresponding author.
*** Corresponding author.
E-mail addresses: reza.tab_chemist@yahoo.com, reza_eivazzadeh@chem.iust.ac.ir (R. Eivazzadeh-Keihan), maleki@iust.ac.ir (A. Maleki), mmheravi@alzahra.ac.ir (M.M. Heravi).

https://doi.org/10.1016/j.heliyon.2024.e39073
Received 19 June 2024; Received in revised form 15 September 2024; Accepted 7 October 2024
Available online 12 October 2024

1. Introduction

Hydrogels are three-dimensional hydrophilic networks that can absorb thousands of times their weight in water due to the presence of hydrophilic functional groups such as -OH, -$CONH_2$, and -SO_3H [1,2]. Hydrogels can have great potential for biomedical purposes due to their hydrophilic nature, biocompatibility, biodegradability, good mechanical strength, and porous structure compared to other biological materials [3]. An important limitation of using hydrogels is their low mechanical strength. For modification this issue, natural hydrogels are gradually being replaced by synthetic hydrogels to achieve higher gel strength, greater water absorption capacity, and longer merit life [2]. Biopolymers hydrogels are a large class of hydrogels that have been widely studied in biomedicine. Biopolymers are natural polymers created of polysaccharides and polypeptides originated from plants and animals. Biomedical hydrogels embedded with biopolymers are of great attention due to their intrinsic biochemical and biophysical features, including cellular stick, degradation, and viscoelasticity. Polysaccharides and polypeptides are two broad categories of biopolymers. Alginates, chitosan, hyaluronic acid, heparin, chitin, chondroitin sulfate, and acacia gum as examples of polysaccharides, and the former includes keratin, albumin, gelatin, elastin, and silk fibroin. The use of particular polysaccharides or polypeptides can induce desirable properties such as cell adhesion or degradability to the hydrogel [4,5].

Acacia gum (AG), commonly called gum arabic (GA), is one of the most important polysaccharides used in biomedicine. It is obtained from the stems and branches of Senegal AG or species close to acacia. It is a water-soluble gum that consists of higher molecular weight polysaccharides and their calcium, potassium, and magnesium salts. The AG comprise arabinose, galactose, rhamnose, and glucuronic acid are produced [6]. In traditional medicine, before these numerous drugs, AG was uesed internally for the treatment of inflammation of the intestinal mucosa, also used to heal damaged and inflamed skin externally. Also, previous research showed that AG has a protective effect against empirical gentamicin, cisplatin nephrotoxicity, doxorubicin cardiotoxicity, and acetaminophen hepatotoxicity in mice [7]. AG has received much attention in biomedicine due to its anti-oxidant properties. For example, it was used in the design of systems for wound healing and cosmetic formulations or sunscreens [8,9]. Specific physico-chemical features and biocompatibility of AG make it a suitable candidate for the preparation of eco-friendly, highly stable and biologically active nanobiocomposites [10].

As mentioned above, silk fibroin (SF) is another of the most specific polypeptides that can impart desirable properties to the hydrogel. SF is one of the most abundant natural derivative polymers with excellent biological performance [11–17]. It is used widely in biomedical due to its high biocompatibility, controllable biodegradability, easy processing, and versatile performance [18–20]. Recently, SF-based materials have been used for gene therapy [21], wound healing [15,22,23] and tissue regeneration [24], hyperthermia therapy [25], and drug delivery systems [26,27].

Another widely used polymer in biomedicine is polyvinyl alcohol (PVA). PVA is a synthetic polymer constructed of vinyl alcohol-co-vinyl acetate with biocompatible, biodegradable, cellular adhesive, water-solubility, gas permeability, electrospinnability, and high mechanical strength properties [28,29]. It is a hydrophilic polymer that can use to produce hydrogels with high biocompatibility, optimum elasticity, and strong mechanical strength [30]. All of these properties make PVA a suitable polymer for biological applications [12,31–33].

So far, many biocomposites based on these natural polymers have been used for different biological applications with different treatment methods. Hyperthermia Cancer therapy is one of the most widely used treatment methods in recent decades [34]. The remarkable sensitivity of magnetic nanoparticles (MNPs) to external magnetic fields, combined with their chemical resilience, low toxicity, and straightforward production methods, has garnered significant interest in recent years [35]. The superparamagnetic properties of these nanoparticles, along with their ability to form stable dispersions and adjust their magnetic characteristics based on size, have led to their widespread application in biological contexts. One notable application is the generation of localized therapeutic heat within tumors, achieved through iron MNP-induced hyperthermia, which operates effectively within the temperature range of 41–46 °C [36]. This technique selectively targets cancer cells while minimizing damage to surrounding healthy tissues, presenting a promising approach for cancer treatment. Consequently, extensive research has been conducted to investigate the potential of MNPs in cancer therapy, among other applications. Magnetic hydrogels, which contain at least one magnetic component, exhibit changes in their properties when subjected to external magnetic fields [37]. Recently, dextran-coated Fe_3O_4 magnetic nanoparticles have been

Table 1
The purity and brand of the materials employed in this study.

Material	CAS No.
AG powder	9000-01-5
$CaCl_2{\cdot}2H_2O$	10035-04–8
LiBr (147.01 Mw)	7550-35-8
Na_2CO_3	497-19-8
Tris base	77-86-1
EDTA	6381-92-6
$FeCl_3{\cdot}6H_2O$	10025-77-1
$FeCl_2{\cdot}4H_2O$	13478-10-9
Ammonia	7664-41-7
Dialysis tubing cellulose membrane	(14000 Da)
Silkworm cocoons	locals
Cisplatin	(Sigma-Aldrich, MO, United States),
MTT (3-(4, 5 dimethylthiazol-2-yl)-2, 5-diphenyl tetrazolium bromide) solution	(Sigma, USA),

Table 2
Details concerning the instruments employed in this investigation.

Instrument	Details of instruments (brand and model)
Fourier Transform Infrared (FT-IR)	Perkin Elmer Spectrum RX1 spectrometer via the KBr pellet method
X-ray diffraction (XRD)	Bruker D8 Advance model
Field-Emission Scanning Electron Microscope (FE-SEM)	TESCAN Mira III model
Energy-dispersive X-ray (EDX)	TESCAN MIRA II SAMX detector
Thermogravimetric analysis (TGA)	BahrSTA 504 under an argon atmosphere at a heating rate of 10 °C/min
Vibrating sample magnetometry (VSM)	LBKFB model magnetic Kashan Kavir (5000 Oe)

synthesized [38], demonstrating excellent dispersion in water, resulting in a magnetic fluid characterized by low toxicity, exceptional stability, and enhanced magnetism—attributes that are crucial for the efficacy of magnetic fluid hyperthermia.

In this research, the novel AG-SF hydrogel/PVA/Fe_3O_4 magnetic nanobiocomposite was prepared for biomedical application. The results demonstrated that the synthesized nanobiocomposite is non-toxic to the healthy HEK293T cell line. Additionally, it exhibited approximately a 22 % reduction in the viability of BT549 breast cancer cells after 72 h, confirming its anti-cancer properties. Thus, this nanobiocomposite shows great potential for in vivo applications. Also, for hyperthermia application, the highest specific absorption rate (SAR) was 93.08 w/g at 100 kHz.

2. Materials and methods

All materials used in this study were sourced with high purity from Merck and Sigma-Aldrich (Table 1). Further, the magnetic nanobiocomposite was successfully synthesized, and a variety of analyses were conducted for its characterization. Information regarding the instruments utilized for characterization has been compiled in Table 2.

2.1. Synthesis of AG-SF hydrogel

Initially, 0.5 g of AG powder was dissolved in 20 mL of distilled water and then calcium chloride solution 0.9 M was added to it and placed under the stirring condition at room temperature for 30 min. Afterward, Sodium carbonate solution (0.06 M) was added to the mixture solution and was stirred for 1h at room temperature. Next, the prepared cross-linked hydrogel was neutralized with HCl (0.01 M) solution. After that, for extraction of SF, three silkworm cocoons were disparted into small fragments. Then, it was heated in sodium carbonate solution (0.21 % w/v) for 2 h (up to a boiling point). In this step, the glue-like sericin proteins were removed from the cocoon pieces. Then, the degummed silk fibers were washed with distilled water several times and dried at room temperature overnight. Henceforth, 10 times the weight of dried degummed silk fibers was determined as the volume used for providing LiBr solution 9.3 M in distilled water and stirred for 2h. The remained LiBr was removed by the dialysis process of the acquired solution. The resulting solution was placed in a cellulose membrane and exposed to distilled water at room temperature for 3 days. In the next step, the combination process of the fabricated hydrogel was carried out using the extracted SF solution. For this purpose, 6 mL of the AG hydrogel solution was mixed with 6 mL of SF solution and kept under the stirring condition at room temperature for 1h. Hereafter, 6 mL of the mixture solution (AG-SF hydrogel) was separated to the other step and the rest of it was used for the freeze-drying process. In order to perform the freeze-drying process, the obtained mixture solution was kept in the freezer (−70 °C) for 24 h. After that, the frozen solution was placed into the freeze-dryer device (−60 °C and 0.1 bar pressure) for 24 h.

2.2. Preparation of AG-SF hydrogel/PVA/Fe_3O_4 nanobiocomposite scaffold

In this step, a solution of 0.05 (wt%) of PVA was provided and added to 1 mL of the mixture solution (AG-SF hydrogel) and stirred for 1h at room temperature. For magnetization of prepared nanobiocomposite, in a round flask bottom, 0.97 g of $FeCl_3.6H_2O$ and 0.44 g of $FeCl_2.4H_2O$ were dissolved at 50 mL of distilled water and were added to 6 mL of AG-SF hydrogel/PVA nanobiocomposite solution. Then, the mixture solution was kept under the stirring condition and N_2 atmosphere at 70 °C. Next, 10 mL of ammonia solution (25 %) was added drop by drop to the mixture solution during the 30 min and stirred for 2 h. Hereafter, the obtained black precipitation was separated by an external magnet and was washed several times to receive pH = 7. Finally, the prepared precipitation was dried in an oven ($80^{\circ}C$) overnight.

2.3. Biocompatibility assay

MTT assay was used to determine the toxicity and biocompatibility of the AG-SF hydrogel/PVA/Fe_3O_4 nanobiocomposite. First, the breast cancer cells line (BT549 cells) and human embryonic kidney cells line (HEK293T cells) were prepared at the Pasteur Institute of Iran. Next, the proper culture medium containing DMEM/F12, 10 % fetal bovine serum (FBS), and 1 % pen-strep was prepared and the cells were cultured at 5×10^3 cell/well in a 96 well plate. Then, serially dilutions of nanobiocomposite (0.015, 0.031, 0.062, 0.125, 0.25, 0.5, 0.75, 1, 1.25, 1.5, 1.75 mg/mL) were added to each well and incubated for 48 h and 72 h. Also, Cisplatin and the culture medium without any additive was used as the positive and negative controls, respectively. In the next step, the cells were treated with MTT (3-(4, 5 dimethylthiazol-2-yl)-2, 5-diphenyl tetrazolium bromide) solution and incubated for 4 h at 37 °C. Next, 1 % SDS was

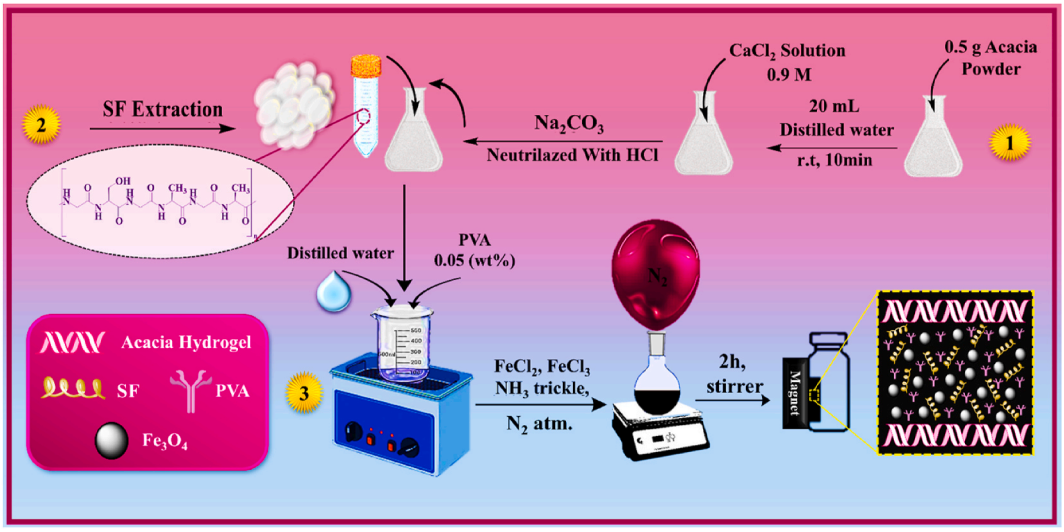

Scheme 1. Synthetic process of the scaffold AG-SF hydrogel/PVA/Fe_3O_4 nanobiocomposite.

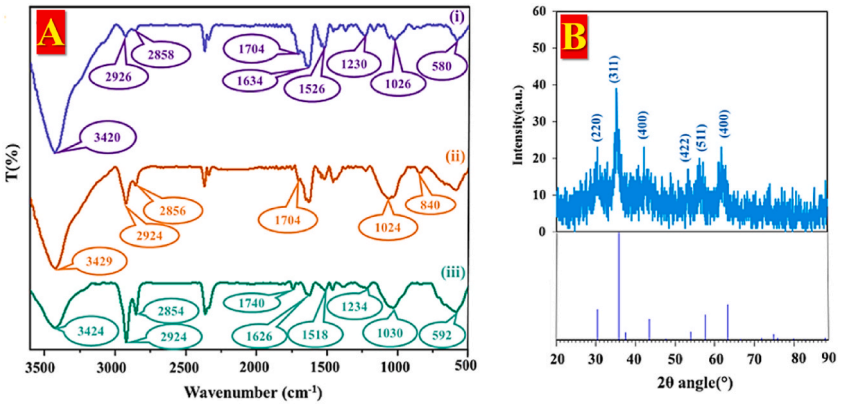

Fig. 1. (A) FT-IR (i) AG-SF hydrogel, (ii) AG-SF hydrogel/PVA, and (iii) AG-SF hydrogel/PVA/Fe_3O_4 magnetic nanobiocomposite. (B) X-ray diffraction patterns of prepared nanobiocomposite.

added to the wells and incubated for 16 h at 37 °C. Finally, the optical density of samples was measured at 550 nm utilizing a microplate reader spectrophotometer (BioTeK, USA). All tests were done in duplicate [3]. The percentage of toxicity and cell viability was calculated according to the following formulas [12]:

Eq. (1):

$$Toxicity\ \% = \left(1 - \frac{mean\ OD\ of\ sample}{mean\ OD\ of\ negative\ control}\right) \times 100$$

Eq. (2):

$$Viability\ \% = 100 - Toxicity\ \%$$

3. Result and discussion

In the present study, according to medical strategies in various cancer treatment methods and new approaches to improve the treatment conditions, a novel nanobiocomposite scaffold AG-SF hydrogel/PVA/Fe_3O_4 was designed and synthesized. AG hydrogel was synthesized by a facile method and modified with extracted natural protein SF and water-soluble synthetic polymer PVA. Finally, it was magnetized with Fe_3O_4 MNP for use in hyperthermia cancer therapy. All of the synthesized steps showed as well in Scheme 1. The cytotoxicity effect of the prepared biocompatible scaffold was investigated in the presence of a breast cancer cell line (BT549 cells). In addition, various spectral and analytical detection techniques were used to prove the synthesis and characterization of the prepared nanobiocomposite structure. Therefore, FT-IR analysis was performed to identify the functional groups and the presence of new

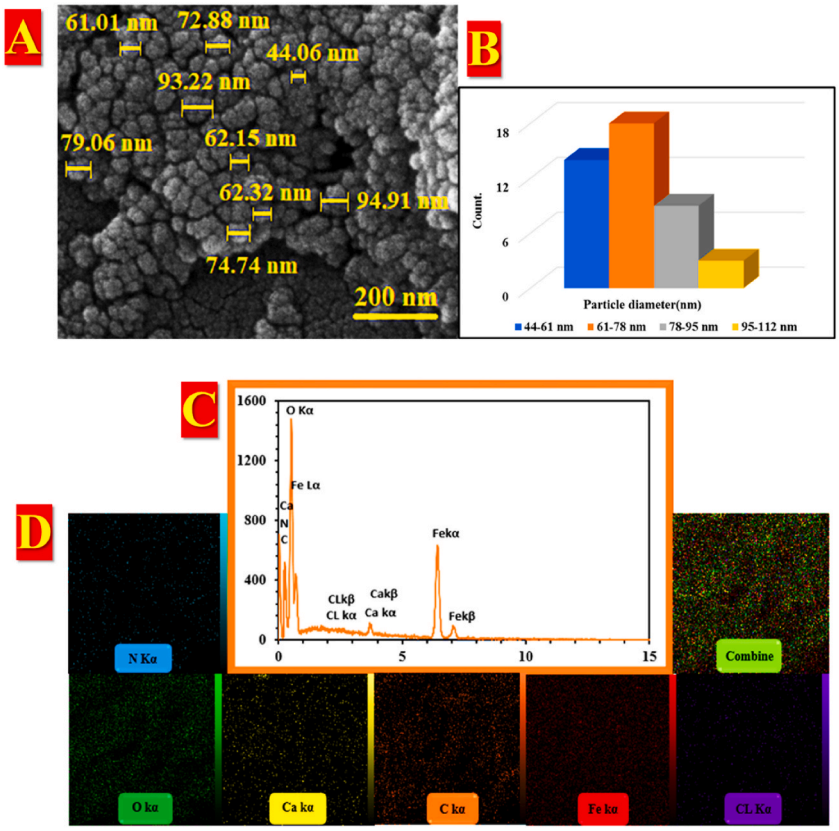

Fig. 2. FE-SEM image in magnification 200 nm (A), the particle size histogram (B), EDX spectrum (C) and EDX mapping images (D) of AG-SF hydrogel/PVA/Fe_3O_4 magnetic nanobiocomposite.

chemical bonds. XRD analysis was done to identify the crystalline phase of Fe_3O_4 MNP. Also, other analyses such as EDX, FE-SEM, TGA, and VSM were performed to evaluate the structural elements, morphology, thermal stability, and magnetic properties. Finally, the efficiency and performance of this nanobiocomposite for hyperthermia method were evaluated by an alternating magnetic field (AFM) as a targeted heating therapy system.

3.1. Fourier transform infrared spectroscopy (FT-IR) and X-ray diffraction (XRD)

To study the presence of necessary functional groups in the structure of the scaffold, FT-IR spectra of the AG-SF hydrogel (spectrum i), AG-SF hydrogel/PVA nanobiocomposite (spectrum ii), and scaffold AG-SF hydrogel/PVA/Fe_3O_4 nanobiocomposite (spectrum iii) were acquired and are presented in Fig. 1A. Pellets containing 0.1–1.0 % of the samples were mixed with 200–250 mg of KBr powder for analysis. The Fourier-transform infrared (FT-IR) spectrometer (PerkinElmer Spectrum RX1) was utilized to characterize functional groups at each synthesis stage. The spectra were recorded with a resolution of 4 cm−1 over a frequency range of 400–4000 cm−1. The average number of readings varied from 6 to 18, and all spectra were obtained at ambient temperature. As can be seen, the peaks that appeared at ~3420 cm^{-1}, ~2926 cm^{-1}, ~ 1024 cm^{-1}, and ~1230 cm^{-1} were attributed to the presence of the O−H, C−H, and C−O bands in AG hydrogel structure, respectively. Also, an absorption peak appeared at ~1704 cm^{-1} that can be attributed to C=O groups in the structure of the AG. The three vibrational bands in different FT-IR regions such as ~1230 cm^{-1}, ~1522 cm^{-1},and ~1630 cm^{-1} were attributed C−N stretching vibration mode of amide III, N−H bending vibration mode of amide II, C=O stretching vibration mode of amide I that proved the presence of SF chains in nanobiocomposite structure. The bands between ~480–660 cm^{-1} were attributed to the vibrations mode of pyranose rings (Fig. 1A (i)) [39]. In Fig. 1A (ii) spectrum, all of the absorption peaks attributed to AG-SF hydrogel were observed. In addition, an absorption peak was attributed to the vibration stretching of C−C in the alkyl chain backbone of the PVA polymer structure appeared at~ 840 cm^{-1}. The stretching vibration of C−O, C=O, C−H, and O−H bands in PVA structure were appeared at ~1024 cm^{-1}, ~1704 cm^{-1}, ~ 2924 cm^{-1}, ~2856 cm^{-1} and ~3429 cm^{-1}, respectively which overlapped with the stretching vibration of C=O, C−H, and O−H bands C=O, C−H, and O−H bands at AG hydrogel structure [40]. Fig. 1A (iii) showed the FT-IR spectrum of AG-SF hydrogel/PVA magnetized with Fe_3O_4 nanoparticles. The absorption peak related to stretching vibration of Fe−O band appeared at ~592 cm^{-1} [41,42].

The XRD pattern of the scaffold AG-SF hydrogel/PVA/Fe_3O_4 nanobiocomposite was exhibited in Fig. 1B. This instrument was equipped with a Lynxeye detector (0D mode) and utilized Cu-Kα radiation (λ = 0.154 nm, 40 kV, 40 mA). A scanning angle of $5° \leq 2\theta$

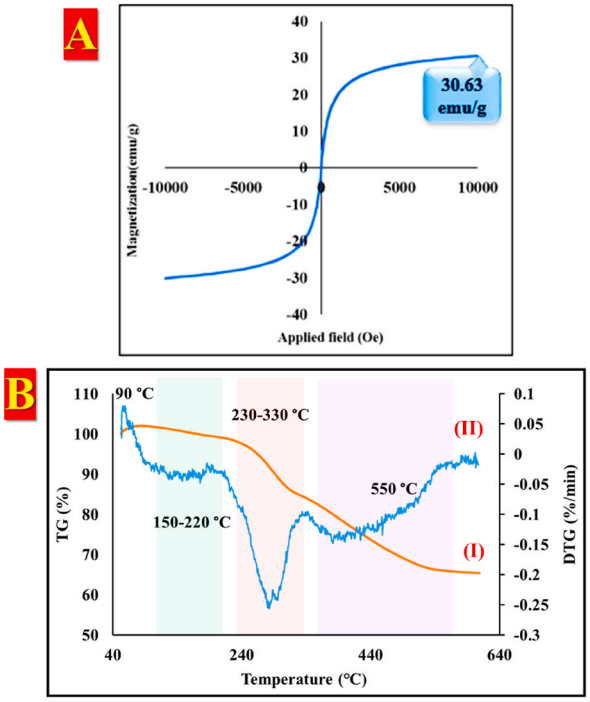

Fig. 3. Room-temperature *M–H* curves (VSM) (A), Thermogravimetric (TGA) (B(I)) and Differential thermogravimetric (DTG) (B (II)) curves of the AG-SF hydrogel/PVA/Fe_3O_4 nanobiocomposite scaffold.

$\leq 90°$ was employed, with a scanning rate of 0.2°/s. As shown, the crystalline phase of Fe_3O_4 MNP was well defined. The XRD pattern displayed the diffraction peaks at 30.26, 35.59, 43.32, 53.64, 57.23, and 62.85 pertained to the lattice planes (220), (311), (400), (422), (511), (440) for Fe_3O_4 nanoparticles (JCPDS No.01-075-0449) [43].

3.2. Field-emission scanning microscopy and energy-dispersed X-ray spectroscopy

The structure of the AG-SF hydrogel/PVA/Fe_3O_4 magnetic nanobiocomposite was examined by a field emission scanning electron microscope, shown in Fig. 2A, B. The sample was secured to a stainless-steel fragment using double-sided carbon tape and subsequently underwent gold sputter coating using an Agar Sputter Coater (model from Agar Scientific, England). The obtained images showed that the synthesized nanobiocomposite has a sphere shape. AG hydrogel has a porous structure, which becomes less porous after being modified with SF and PVA. Finally, the Fe_3O_4 MNPs are placed on the surface and inside the channels to create a circular shape (Fig. 2A). Based on the particle size histogram, the fabricated nanobiocomposite had a homogeneous shape and most of the particles had a size between 47 and 68 nm (Fig. 2B).

EDX analysis was used as a qualitative detection technique for the structural elements of the prepared nanobiocomposite and the results are well shown in Fig. 2C. The TESCAN MIRA II is a high-resolution Scanning Electron Microscope (SEM) that integrates SEM imaging with Energy Dispersive X-ray (EDX) analysis using the SAMX detector, enabling detailed morphological and elemental composition analysis. This combination allows for fast data acquisition and versatile imaging modes, making it efficient for materials characterization and research applications in fields such as material science and nanotechnology. As observed, the calcium peak proved the presence of calcium ions as a cross-linking agent. The presence of associated organic structures including biopolymer AG and SF protein was confirmed by observing three strong peaks of carbon, nitrogen, and oxygen. The observed iron peak is also related to the iron oxide nanoparticles in the composite structure. In addition, the presence of partial chlorine peaks can be attributed to the low amount of chlorine ions trapped in the structure of the synthesized nanobiocomposite scaffold. Also, the distribution of these elements was well illustrated by the element mapping images in Fig. 2D.

3.3. Vibrating-sample magnetometer and thermogravimetric analysis

Magnetic property of the produced nanobiocomposite was perused and its results were shown in Fig. 3A. There are considerable factors that can affect the magnetic property. For example, intraparticle and interparticle interactions, nucleus size, and crystal structure of the iron group are very important factors in changing the magnetic property. The magnetization hysteresis loops of AG-SF hydrogel/PVA/Fe_3O_4 nanobiocomposite have S-like curves. As can be seen, the saturation magnetization amounts diminished until 30.63 emu/g after composition to AG-SF hydrogel/PVA compared with the amount of saturated magnetic Fe_3O_4 MNP [44].

To study thermal stability of AG-SF hydrogel/PVA/Fe_3O_4 nanobiocomposite scaffold, TGA analysis was implemented in a thermal

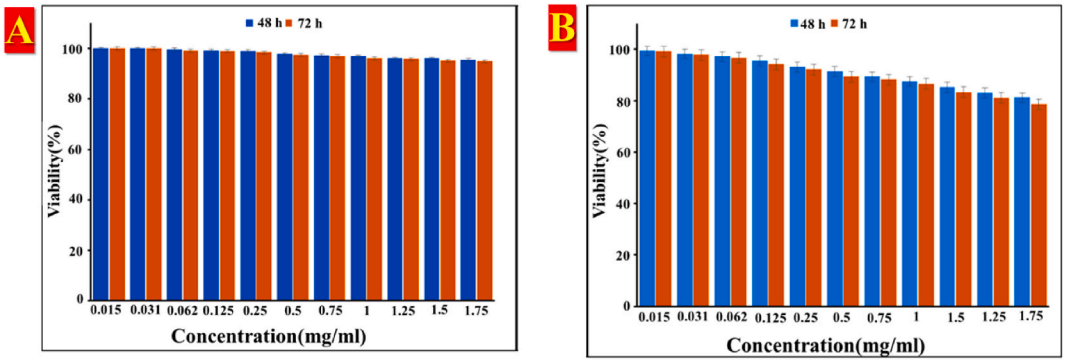

Fig. 4. Cell viability of AG-SF hydrogel/PVA/Fe_3O_4 nanobiocomposite against HEK293T (A) and (B) BT549 cell line after 48 h and 72 h of prepared nanocomposite.

range of 50–600 °C (Fig. 3B). As can be seen, initially, with increasing temperature, and increasing peak (1 %) was observed up to 90 °C, which is due to the buoyancy effect of the instrument [45]. After that, the prepared nanobiocomposite with three reducing peaks lost 32 % of its weight. Up the temperature to 150 °C–220 °C, the first weight loss (2 %) happened that was attributed to the decomposition of water molecules trapped in the nanobiocomposite structure. The second weight loss (13 %) appeared at 230°C–330 °C .In this stage, polysaccharide chains of AG hydrogel and synthesize polymer were decomposed [46]. Afterward, by increasing the temperature to 550 °C, the weight of the prepared nanobiocomposite was reduced (18 %). SF protein chains were decomposed in this temperature range [47]. All the organic compounds in the structure were decomposed to this temperature. All these findings were also confirmed by the DTG curve analysis, which provided clear peaks corresponding to the weight loss events observed in the TGA. The DTG curve indicated the rates of mass loss at specific temperature ranges, aligning with the identified decomposition stages of water, polysaccharide chains, and SF protein. This correlation between the TGA and DTG results enhances the reliability of the thermal stability data for the AG-SF hydrogel/PVA/Fe3O4 nanobiocomposite scaffold.

3.4. MTT assay

The results showed that the viability percentage of HEK293T cells did not change significantly after 48 h and 72 h, and therefore the synthesized AG-SF hydrogel/PVA/Fe_3O_4 nanobiocomposite is not toxic to this cell line (Fig. 4A). At the same time, the synthesized AG-SF hydrogel/PVA/Fe_3O_4 nanobiocomposite exhibits approximately a 22 % decrease in cell viability of BT549 cells at 1.75 mg/mL concentration after 72 h (Fig. 4B). Therefore, it can be said that this nanobiocomposite has anti-cancer properties against the BT549 breast cancer cell line.

3.5. Hyperthermia application

Cancer is one of the leading causes of mortality worldwide, and its prevalence is increasing more and more. Current therapies are inadequate and include numerous limitations. It has long been known that hyperthermia may be used to treat cancer, primarily in cases with surface tumors. More recently, the idea of "intracellular hyperthermia" (42–45 °C) has been proposed, in which magnetic particles are focused at the tumor location and remotely heated using an applied magnetic field. Magnetic nanoparticles (MNPs) have wide magnetic moments and high ratios of surface area to volume, which makes them well for treating cancer with hyperthermia and delivering drugs in a controlled way(2). With magnetic nanoparticle-mediated intracellular hyperthermia, it is possible to heat a tumor in a specific place with few unfavorable side effects. After directing magnetic nanoparticles to the tumor tissue, an external alternating magnetic field is used to heat the nanoparticles through a process called Néel relaxation loss. The temperature in tumor tissue is increased to above 43 °C, which causes necrosis of cancer cells but does not damage surrounding normal tissue. In magnetic hyperthermia, stimulation creates heat through three different processes: Néel relaxation, Brownian relaxation, and hysteresis loss. The relative contribution of each is dependent on the shape, crystalline anisotropy, size, and degree of aggregation of the nanoparticles (4). It might be possible to find a critical size for a nanoparticle above which hysteresis loss has a big effect. Below this crucial point, relaxation processes that because the magnetic moment to spin when subjected to a magnetic field would predominate. Néel Relaxation will let heat escape if the magnetization rotates while the particle stays stationary. Otherwise, the particle rotates and the magnetic moment stays constant with the crystallographic axes through which the particle experiences Brownian relaxation. The specific absorption ratio (SAR), which is the rate of heat production, is used to measure the heating efficiency of MNPs.

Eq. (3):

$$\mathrm{SAR} = \frac{C}{m}\frac{\Delta T}{\Delta t}$$

where C is the specific heating capacity of the fluid, m is the concentration of MNPs and ΔT is the temperature change in the time span Δt.

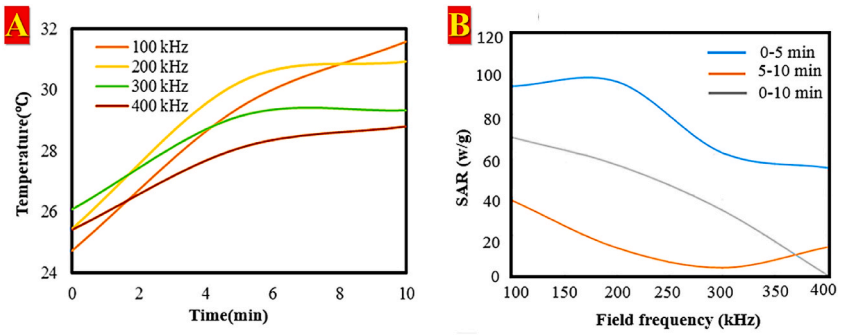

Fig. 5. Heating profile (A) and SAR (B) of AG-SF hydrogel/PVA/Fe_3O_4 magnetic nanobiocomposite with concentration of 1 mg/mL in various field frequencies and different time intervals, respectively.

Experiments were carried out in this study to determine the heating profiles of AG-SF hydrogel/PVA/Fe_3O_4 magnetic nanobiocomposite. An oscillating magnetic field was applied to several samples with concentrations of 1 mg/mL and an initial temperature of the surrounding fluid of 24 °C. To find out how field frequency affects things, different field frequencies of 100 kHz, 200 kHz, 300 kHz, and 400 kHz were used with constant field intensities. During the 10 min of exposure, the temperature of the fluid around the object was checked every 5 min, giving two separate periods. As seen in Fig. 5A, As soon as the magnetic field was applied, the temperature rose dramatically. At 300 kHz, which is 2.96 °C, the temperature goes up the most in the first period. For 100 kHz, 200 kHz, and 400 kHz, the values are 0.71 °C, 1.43 °C, and 2.15 °C, respectively. As a result, the temperature rises as the field frequency increases in the first 5 min. In the second period, however, the field frequency of 200 kHz accounts for the highest temperature rise of 6.23 °C, while the lowest value was measured at 1.45 °C at 400 kHz. The maximum temperature across the whole time frame is 31.57 °C at the field frequency of 100 kHz; hence, the most heat was created over the 10 min of exposure time at 200 kHz.

The SAR is proportional to the rate of temperature change or the slope of the lines in Fig. 5A since the sole variable factor in the aforementioned equation is $\Delta T/\Delta t$. Because there are two time periods, each example may have two SAR values computed. Fig. 5B shows the SAR values for two different times as a function of the field frequency. Due to its steeper graph, it is predicted that the first time interval at 300 kHz will provide the highest value of SAR. As the field frequency rises, the SAR values in the first time interval at 100 kHz, 200 kHz, 300 kHz, and 400 kHz are 93.08 (W/g), 96 (W/g), 61 (W/g), and 53.6 (W/g), respectively. The SAR are 37.4, 13.8, 4, and 14.2(W/g) correspondingly for field frequencies of 100 kHz, 200 kHz, 300 kHz, and 400 kHz at the second period. The highest SAR that can be obtained in this experiment is 93.08 w/g at 100 kHz, which is higher than the one that occurs in the first 5 min at 300 kHz. For the first, second, and whole time intervals, the mean values of SAR are computed as 76.1 (W/g), 17.35 (W/g), and 47.47(W/g), respectively.

4. Conclusions

In this research work, a novel and potent magnetic nanobiocomposite was developed using biocompatible and low-toxicity materials such as AG hydrogel, natural protein silk fibroin, and polyvinyl alcohol. This nanobiocomposite provides an effective scaffold for cancer treatment. The three-dimensional structure of the AG hydrogel was achieved by cross-linking polysaccharide filaments with calcium ions. Subsequently, the hydrogel was modified with silk fibroin and PVA to enhance its biological properties. Various analytical techniques, including FT-IR, EDX, FE-SEM, XRD, TGA, and VSM, were employed to characterize the structure of the prepared nanobiocomposite. The MTT assay demonstrated that the nanobiocomposite exhibited excellent biocompatibility while significantly reducing the growth rate, proliferation, and survival of BT549 cancer cells. These promising biological results underscore the potential of the developed nanobiocomposite for in vivo applications in cancer therapy. Moreover, the study of hyperthermia application using the AG-SF hydrogel/PVA/Fe3O4 magnetic nanobiocomposite yielded compelling results. The Specific Absorption Rate (SAR) was measured at 93.08 W/g at a frequency of 100 kHz. Therefore, this work contributes new insights into the use of this nanobiocomposite for hyperthermia cancer therapy and biological activities.

CRediT authorship contribution statement

Zeinab Pajoum: Writing – review & editing, Investigation, Formal analysis. **Hooman Aghamirza Moghim Aliabadi:** Writing – review & editing, Formal analysis, Data curation. **Adibeh Mohammadi:** Writing – review & editing, Writing – original draft, Formal analysis. **Zahra Sadat:** Writing – review & editing, Writing – original draft, Investigation, Data curation. **Amir Kashtiaray:** Writing – review & editing, Investigation. **Milad Salimi Bani:** Writing – review & editing, Formal analysis, Data curation. **Mohammadali Shahiri:** Investigation, Formal analysis. **Mohammad Mahdavi:** Writing – review & editing, Validation, Data curation. **Reza Eivazzadeh-Keihan:** Writing – review & editing, Writing – original draft, Validation, Formal analysis, Data curation. **Ali Maleki:** Writing – review & editing, Writing – original draft, Validation, Data curation. **Majid M. Heravi:** Writing – review & editing, Validation, Data curation.

Declaration of competing interest

The authors declare that they have no known competing financial interests or personal relationships that could have appeared to influence the work reported in this paper.

Acknowledgement

The authors gratefully acknowledge the partial support from the Research Council of the Iran University of Science (IUST).

References

[1] N. Singh, S. Agarwal, A. Jain, S. Khan, 3-Dimensional cross linked hydrophilic polymeric network "hydrogels": an agriculture boom, Agric. Water Manag. 253 (2021) 106939.
[2] A.S. Hoffman, Hydrogels for biomedical applications, Adv. Drug Deliv. Rev. 64 (2012) 18–23.
[3] R. Eivazzadeh-Keihan, Z. Sadat, H. Aghamirza Moghim Aliabadi, F. Ganjali, A. Kashtiaray, M. Salimi Bani, S. Komijani, M.M. Ahadian, N. Salehpour, R. Ahangari Cohan, Fabrication of a magnetic alginate-silk fibroin hydrogel, containing halloysite nanotubes as a novel nanocomposite for biological and hyperthermia applications, Sci. Rep. 12 (2022) 15431.
[4] R. Eivazzadeh-Keihan, S. Rahmati, Z. Sadat, F. Ganjali, H.A.M. Aliabadi, A. Kashtiaray, A. Maleki, Purification of alkaline phosphatase from bovine milk through metal ion affinity by a novel magnetic nanocomposite based on functionalized chitosan with dopamine and nickel, Mater. Today Commun. 34 (2023) 105461.
[5] Q. Chai, Y. Jiao, X. Yu, Hydrogels for biomedical applications: their characteristics and the mechanisms behind them, Gels 3 (2017) 6.
[6] C. Sanchez, M. Nigen, V.M. Tamayo, T. Doco, P. Williams, C. Amine, D. Renard, Acacia gum: history of the future, Food Hydrocoll 78 (2018) 140–160.
[7] B.H. Ali, A. Ziada, G. Blunden, Biological effects of gum Arabic: a review of some recent research, Food Chem. Toxicol. 47 (2009) 1–8.
[8] B. Singh, S. Sharma, A. Dhiman, Acacia gum polysaccharide based hydrogel wound dressings: synthesis, characterization, drug delivery and biomedical properties, Carbohydr. Polym. 165 (2017) 294–303.
[9] V.P. Padmanabhan, S. Balakrishnan, R. Kulandaivelu, S.N. Tsn, M. Lakshmipathy, S. Sagadevan, F. Mohammad, H.A. Al-Lohedan, S. Paiman, W.C. Oh, Nanoformulations of core–shell type hydroxyapatite-coated gum acacia with enhanced bioactivity and controlled drug delivery for biomedical applications, New J. Chem. 44 (2020) 7175–7185.
[10] S.K.R. Namasivayam, A.M. Rabel, R. Prasana, R.A. Bharani, C.V. Nachiyar, Gum acacia PEG iron oxide nanocomposite (GA-PEG-IONC) induced pharmacotherapeutic activity on the Las R gene expression of Pseudomonas aeruginosa and HOXB13 expression of prostate cancer (Pc 3) cell line. A green therapeutic approach of molecular mechanism inhibition, Int. J. Biol. Macromol. 190 (2021) 940–959.
[11] R. Eivazzadeh-Keihan, F. Radinekiyan, H. Madanchi, H.A.M. Aliabadi, A. Maleki, Graphene oxide/alginate/silk fibroin composite as a novel bionanostructure with improved blood compatibility, less toxicity and enhanced mechanical properties, Carbohydr. Polym. 248 (2020) 116802.
[12] R. Eivazzadeh-Keihan, F. Khalili, H.A.M. Aliabadi, A. Maleki, H. Madanchi, E.Z. Ziabari, M.S. Bani, Alginate hydrogel-polyvinyl alcohol/silk fibroin/magnesium hydroxide nanorods: a novel scaffold with biological and antibacterial activity and improved mechanical properties, Int. J. Biol. Macromol. 162 (2020) 1959–1971.
[13] D.-M. Radulescu, V.-A. Surdu, A. Ficai, D. Ficai, A.-M. Grumezescu, E. Andronescu, Green synthesis of metal and metal oxide nanoparticles: a review of the principles and biomedical applications, Int. J. Biol. Macromol. 24 (2023) 15397.
[14] P. Figueiredo, K. Lintinen, J.T. Hirvonen, M.A. Kostiainen, H.A. Santos, Properties and chemical modifications of lignin: towards lignin-based nanomaterials for biomedical applications, Prog. Mater. Sci. 93 (2018) 233–269.
[15] R. Eivazzadeh-Keihan, H.A.M. Aliabadi, F. Radinekiyan, M. Sobhani, A. Maleki, H. Madanchi, M. Mahdavi, A.E. Shalan, Investigation of the biological activity, mechanical properties and wound healing application of a novel scaffold based on lignin–agarose hydrogel and silk fibroin embedded zinc chromite nanoparticles, RSC adv 11 (2021) 17914–17923.
[16] R. Eivazzadeh-Keihan, E.B. Noruzi, H.A.M. Aliabadi, S. Sheikhaleslami, A.R. Akbarzadeh, S.M. Hashemi, M.G. Gorab, A. Maleki, R.A. Cohan, M. Mahdavi, Recent advances on biomedical applications of pectin-containing biomaterials, Int. J. Biol. Macromol. 217 (2022) 1–18.
[17] R. Eivazzadeh-Keihan, L. Choopani, H.A.M. Aliabadi, F. Ganjali, A. Kashtiaray, A. Maleki, R.A. Cohan, M.S. Bani, S. Komijani, M.M. Ahadian, Magnetic carboxymethyl cellulose/silk fibroin hydrogel embedded with halloysite nanotubes as a biocompatible nanobiocomposite with hyperthermia application, Mater. Chem. Phys. 287 (2022) 126347.
[18] T.P. Nguyen, Q.V. Nguyen, V.-H. Nguyen, T.-H. Le, V.Q.N. Huynh, D.-V.N. Vo, Q.T. Trinh, S.Y. Kim, Q.V. Le, Silk fibroin-based biomaterials for biomedical applications: a review, Polymers 11 (2019) 1933.
[19] R. Eivazzadeh-Keihan, F. Radinekiyan, H.A.M. Aliabadi, S. Sukhtezari, B. Tahmasebi, A. Maleki, H. Madanchi, Chitosan hydrogel/silk fibroin/Mg (OH) 2 nanobiocomposite as a novel scaffold with antimicrobial activity and improved mechanical properties, Sci. Rep. 11 (2021) 650.
[20] R. Eivazzadeh-Keihan, F. Ahmadpour, H.A.M. Aliabadi, F. Radinekiyan, A. Maleki, H. Madanchi, M. Mahdavi, A.E. Shalan, S. Lanceros-Méndez, Pectin-cellulose hydrogel, silk fibroin and magnesium hydroxide nanoparticles hybrid nanocomposites for biomedical applications, Int. J. Biol. Macromol. 192 (2021) 7–15.
[21] M.A. Tomeh, R. Hadianamrei, X. Zhao, Silk fibroin as a functional biomaterial for drug and gene delivery, Pharm. Times 11 (2019) 494.
[22] L.-D. Koh, J. Yeo, Y.Y. Lee, Q. Ong, M. Han, B.C. Tee, Advancing the frontiers of silk fibroin protein-based materials for futuristic electronics and clinical wound-healing (Invited review), Mater. Sci. Eng. C 86 (2018) 151–172.
[23] R. Eivazzadeh-Keihan, F. Khalili, N. Khosropour, H.A.M. Aliabadi, F. Radinekiyan, S. Sukhtezari, A. Maleki, H. Madanchi, M.R. Hamblin, M. Mahdavi, Hybrid bionanocomposite containing magnesium hydroxide nanoparticles embedded in a carboxymethyl cellulose hydrogel plus silk fibroin as a scaffold for wound dressing applications, ACS Appl. Mater. Interfaces 13 (2021) 33840–33849.
[24] A.S. Gobin, V.E. Froude, A.B. Mathur, Structural and mechanical characteristics of silk fibroin and chitosan blend scaffolds for tissue regeneration, J. Biomed. Mater. Res. 74 (2005) 465–473.
[25] K.-Y. Qian, Y. Song, X. Yan, L. Dong, J. Xue, Y. Xu, B. Wang, B. Cao, Q. Hou, W. Peng, Injectable ferrimagnetic silk fibroin hydrogel for magnetic hyperthermia ablation of deep tumor, Biomater 259 (2020) 120299.
[26] F. Mottaghitalab, M. Farokhi, M.A. Shokrgozar, F. Atyabi, H. Hosseinkhani, Silk fibroin nanoparticle as a novel drug delivery system, J. Control. Release. 206 (2015) 161–176.
[27] S.U.D. Wani, S.P. Gautam, Z.L. Qadrie, H. Gangadharappa, Silk fibroin as a natural polymeric based bio-material for tissue engineering and drug delivery systems-A review, Int. J. Biol. Macromol. 163 (2020) 2145–2161.
[28] W.A. Abbas, I.M. Sharafeldin, M.M. Omar, N.K. Allam, Novel mineralized electrospun chitosan/PVA/TiO 2 nanofibrous composites for potential biomedical applications: computational and experimental insights, Nanoscale Adv. 2 (2020) 1512–1522.
[29] R. Eivazzadeh-Keihan, Z. Pajoum, H.A.M. Aliabadi, A. Mohammadi, A. Kashtiaray, M.S. Bani, B. Pishva, A. Maleki, M.M. Heravi, M. Mahdavi, Magnetized chitosan hydrogel and silk fibroin, reinforced with PVA: a novel nanobiocomposite for biomedical and hyperthermia applications, RSC adv 13 (2023) 8540–8550.
[30] A. Hashim, H. Abduljalil, H. Ahmed, Fabrication and characterization of (PVA-TiO2) 1-x/SiCx nanocomposites for biomedical applications, Egypt, J. Chem. 63 (2020) 71–83.
[31] M.S.B. Husain, A. Gupta, B.Y. Alashwal, S. Sharma, Synthesis of PVA/PVP based hydrogel for biomedical applications: a review, Energ. source part A 40 (2018) 2388–2393.

[32] E.A. Kamoun, S.A. Loutfy, Y. Hussein, E.-R.S. Kenawy, Recent advances in PVA-polysaccharide based hydrogels and electrospun nanofibers in biomedical applications: a review, Int. J. Biol. Macromol. 187 (2021) 755–768.
[33] M. Chozhanathmisra, L. Murugesan, A. Murugesan, G. Palanisamy, R. Rajavel, Enhancement on physical, chemical, and biological properties of HNT-PVA-ALG-HAp biocomposite coating on implant substrate for biomedical application, Ceram. Int. 48 (2022) 16868–16876.
[34] N. Naderi, F. Lalebeigi, Z. Sadat, R. Eivazzadeh-Keihan, A. Maleki, M. Mahdavi, 1Recent advances on hyperthermia therapy applications of carbon-based nanocomposites, Colloids Surf. B Biointerfaces (2023) 113430.
[35] R. Eivazzadeh-Keihan, S. Bahrami, M. Ghafori Gorab, Z. Sadat, A. Maleki, Functionalization of magnetic nanoparticles by creatine as a novel and efficient catalyst for the green synthesis of 2-amino-4H-chromene derivatives, Sci. Rep. 12 (2022) 10664.
[36] Z. Sadat, A. Kashtiaray, F. Ganjali, H.A.M. Aliabadi, N. Naderi, M.S. Bani, S. Shojaei, R. Eivazzadeh-Keihan, A. Maleki, M. Mahdavi, Production of a magnetic nanocomposite for biological and hyperthermia applications based on chitosan-silk fibroin hydrogel incorporated with carbon nitride, Int. J. Biol. Macromol. 279 (2024) 135052.
[37] R. Eivazzadeh-Keihan, Z. Pajoum, H.A.M. Aliabadi, F. Ganjali, A. Kashtiaray, M.S. Bani, F. Lalebeigi, E.Z. Ziabari, A. Maleki, M.M. Heravi, Magnetic chitosan-silk fibroin hydrogel/graphene oxide nanobiocomposite for biological and hyperthermia applications, Carbohydrate Polymers 300 (2023) 120246.
[38] H. Li, Q. Wu, X. Yuan, Y. Li, Y. Xu, R. Hong, Preparation of water-based dextran-coated Fe3O4 magnetic fluid for magnetic hyperthermia, Nanotechnol. Rev. 12 (2023) 20220534.
[39] M. Bashir, S. Haripriya, Assessment of physical and structural characteristics of almond gum, Int. J. Biol. Macromol. 93 (2016) 476–482.
[40] A. Kharazmi, N. Faraji, R.M. Hussin, E. Saion, W.M.M. Yunus, K. Behzad, Structural, optical, opto-thermal and thermal properties of ZnS–PVA nanofluids synthesized through a radiolytic approach, Beilstein j. nanotech. 6 (2015) 529–536.
[41] R. Eivazzadeh-Keihan, R. Taheri-Ledari, N. Khosropour, S. Dalvand, A. Maleki, S.M. Mousavi-Khoshdel, H. Sohrabi, Fe3O4/GO@ melamine-ZnO nanocomposite: a promising versatile tool for organic catalysis and electrical capacitance, Colloids Surf. A Physicochem. Eng. Asp. 587 (2020) 124335.
[42] R. Eivazzadeh-Keihan, F. Radinekiyan, A. Maleki, M.S. Bani, Z. Hajizadeh, S. Asgharnasl, A novel biocompatible core-shell magnetic nanocomposite based on cross-linked chitosan hydrogels for in vitro hyperthermia of cancer therapy, Int. J. Biol. Macromol. 140 (2019) 407–414.
[43] S. Chidambaram, B. Pari, N. Kasi, S. Muthusamy, ZnO/Ag heterostructures embedded in Fe3O4 nanoparticles for magnetically recoverable photocatalysis, J. Alloys Compd. 665 (2016) 404–410.
[44] R. Eivazzadeh-Keihan, F. Radinekiyan, A. Maleki, M. Salimi Bani, M. Azizi, A new generation of star polymer: magnetic aromatic polyamides with unique microscopic flower morphology and in vitro hyperthermia of cancer therapy, J. Mater. Sci. 55 (2020) 319–336.
[45] T. Shamsi, A. Amoozadeh, S.M. Sajjadi, E. Tabrizian, Novel type of SO3H–functionalized nano-titanium dioxide as a highly efficient and recyclable heterogeneous nanocatalyst for the synthesis of tetrahydrobenzo [b] pyrans, Appl. Organomet. Chem. 31 (2017) e3636.
[46] C. Cozic, L. Picton, M.-R. Garda, F. Marlhoux, D. Le Cerf, Analysis of Arabic gum: study of degradation and water desorption processes, Food Hydrocoll 23 (2009) 1930–1934.
[47] M.M. Gomaa, C. Hugenschmidt, M. Dickmann, E.E. Abdel-Hady, H.F. Mohamed, M.O. Abdel-Hamed, Crosslinked PVA/SSA proton exchange membranes: correlation between physiochemical properties and free volume determined by positron annihilation spectroscopy, Phys. Chem. Chem. Phys. 20 (2018) 28287–28299.